Journal of Nuclear Materials 377 (2008) 195–200

Contents lists available at ScienceDirect

Journal of Nuclear Materials

journal homepage: www.elsevier.com/locate/jnucmat

Numerical study on pressure wave propagation in a mercury loop

H. Kogawa [a,*], S. Hasegawa [a], M. Futakawa [a], B. Riemer [b], M. Wendel [b], J. Haines [b]

[a] Japan Atomic Energy Agency, 2-4 Shirakata-Shirane, Tokai-mura, Naka-gun, Ibaraki-ken 319-1195, Japan
[b] Oak Ridge National Laboratory, 701 Scarboro Road, Oak Ridge, TN 37830-6474, USA

A B S T R A C T

On-beam tests were carried out at the Los Alamos Neutron Science Center–Weapons Neutron Research (LANSCE–WNR) facility in June 2005 to investigate pressure wave mitigation in mercury targets for the MW-class spallation neutron sources under international collaboration between US Spallation Neutron Source (SNS) and Japanese Spallation Neutron Source (JSNS). A mercury loop was used for the target, a so-called In-Beam Bubbling Test Loop (IBBTL). The loop consists of the rectangular pipe of 25 mm × 50 mm^2 in cross section, 1.5 mm in wall thickness and 2 m in total length approximately. The SNS team set 8 strain sensors on the pipe wall to measure the strain propagation caused by the pressure wave. The maximum strain appeared at 350 mm apart from the proton-bombarded point at 5.5 ms after the proton bombardment. It is known that the propagation velocity of the pressure wave in mercury is ca. 1500 m/s and that of the stress wave in stainless steel is ca. 5000 m/s. However, the apparent wave propagation velocity in the IBBTL was lower than those velocities and was observed to be 65 m/s. Numerical analysis was carried out to understand the strain propagation in the pipe wall of the IBBTL. Numerical results showed that the maximum strain at 350 mm apart from the beam spot appeared at 5.5 ms after proton bombardment in good agreement with experimental results.

1. Introduction

High-intensity pulsed spallation neutron sources are being constructed in Japan and committed in US. In the pulsed spallation neutron sources, pulsed protons bombarded a heavy metal target in a microsecond to produce high-intensity neutrons by the spallation reaction. The neutrons are mainly used for neutron scattering experiments in the materials and life sciences. The Japanese Spallation Neutron Source (JSNS) is one of the facilities in J-PARC (Japan Proton Accelerator Research Complex) constructed by the Japan Atomic Energy Agency (JAEA) and High Energy Accelerator Organization (KEK) [1]. In JSNS, pulsed protons (3 GeV, 1 MW at 25 Hz, 1 μs pulse duration) bombard a liquid mercury target, which has advantages for heat removal due to self circulation and ensures a high neutron yield.

A target vessel made of type 316LN stainless steel (SS316LN) contains the liquid mercury. At the moment the protons hit the mercury target, thermal stress waves occur in the target vessel and pressure waves are generated in the mercury due to the rapid heat deposition [2,3]. Numerical simulations have indicated that the maximum stress in the target vessel due to the pressure waves can reach to 200 MPa [3]. Another consequence of the pressure waves is pitting damage to the vessel as a result of cavitation in mercury [4–9].

It is desired to reduce the pressure wave in order to decrease the pitting damage and the stress in the target vessel. It is suggested that micro-bubbles injection into the mercury is an effective methods to mitigate the pressure waves [10,11]. The micro-bubbles enhance compressibility of mercury and lead to the absorption of the energy of the pressure wave.

Under an international collaboration between JAEA and Oak Ridge National Laboratory (ORNL), on-beam tests were carried out in June 2005 at the Los Alamos Neutron Science Center-Weapons Neutron Research (LANSCE–WNR) facility in Los Alamos National Laboratory (LANL) to verify the effect of the injected micro-bubbles on the pitting damage, the pressure wave and target vessel strain [12]. A loop type target was used and strains caused by the pressure wave were measured. This paper presents numerical analysis carried out in order to understand the strain response due to pressure wave propagation which is affected by the interaction between the liquid metal and the solid structure.

2. Experimental

Fig. 1 shows the photograph of the loop type target, or so-called IBBTL (In-Beam Bubble Test Loop) [12], which was used to investigate the bubbling effect on the pressure waves, pitting damage and vessel strain. The total length of the loop is about 2 m. Mercury is contained and circulated inside a rectangular pipe made of Type 304 stainless steel. A magnetic induction pump drives the mercury

* Corresponding author.
E-mail address: kogawa.hiroyuki@jaea.go.jp (H. Kogawa).

0022-3115/$ - see front matter © 2008 Elsevier B.V. All rights reserved.
doi:10.1016/j.jnucmat.2008.02.078

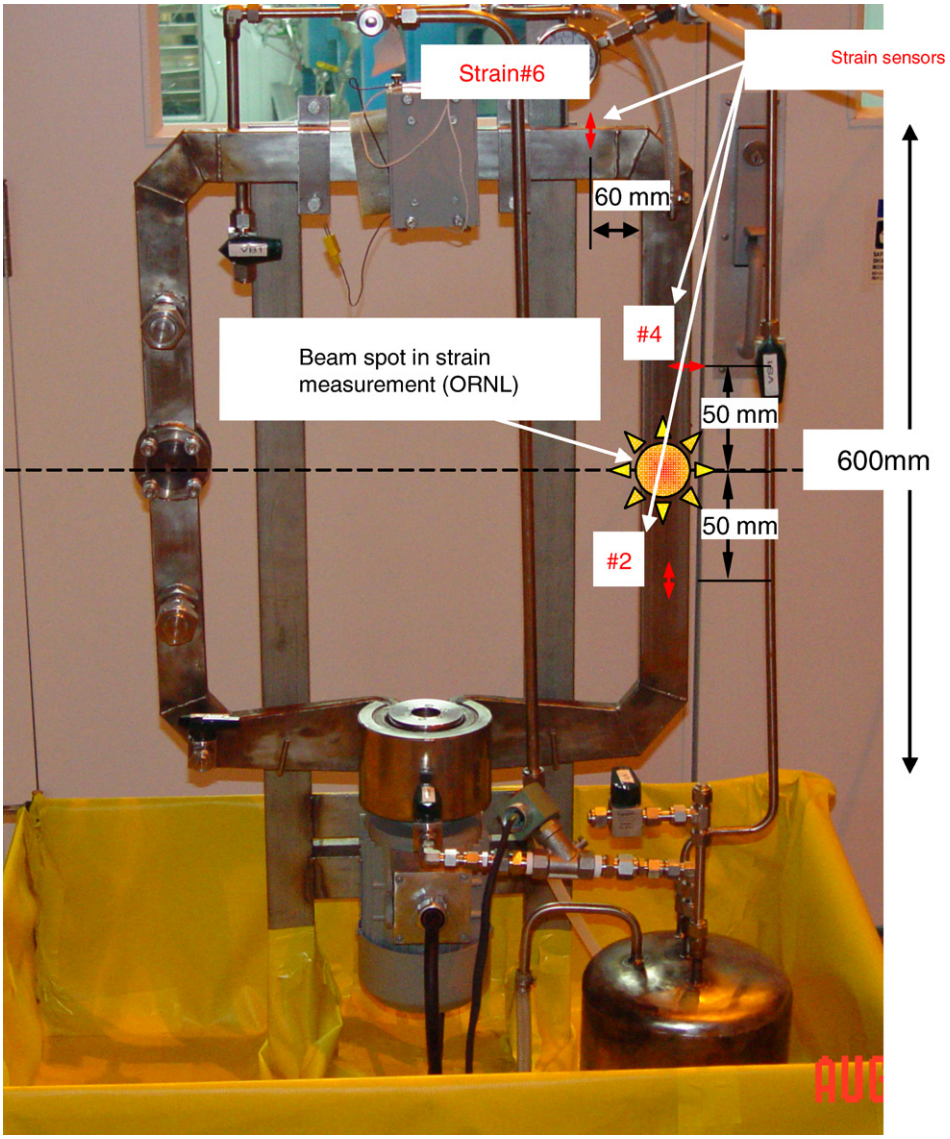

Fig. 1. The In-Beam Bubbling Test Loop (IBBTL) and strain sensors positions [12].

flow in the pipe. The rectangular pipe has the cross section of $50.8 \times 25.4\ mm^2$ with wall thickness of 1.5 mm. Flanges for mounting replaceable damage test specimens (DTS) are placed on the left hand leg of the loop as shown in Fig. 1. In the strain measurement tests, the proton beam bombarded the center of the right hand leg at the indicated 'beam spot' in Fig. 1. The proton energy was 800 MeV for this test and about 2.5×10^{13} protons per pulse were injected into the IBBTL. The beam profile was described by Gaussian distribution with sigma equal to ca. 9 mm and the foot print was circular.

The dynamic strain was measured at eight positions [12]. In Fig. 1, only the three sensor positions discussed in this paper are shown. Sensor #2 was set on the center of the loop at 50 mm apart from the beam spot and oriented to measure loop axis direction. Sensors #4 and #6 were set on the edge of the loop to measure circumferential direction strain at 50 mm and about 350 mm apart from the beam spot, respectively.

3. Numerical analysis

Numerical analyses were carried out to understand the pressure wave propagation behavior by using the explicit Finite Element Method (FEM) code, LS-DYNA [13]. Fig. 2 shows a finite element model of the IBBTL used for the analyses. The analyses were carried out by using a half model of the IBBTL taking the symmetry of the IBBBTL into account. The pipe wall and the DTS were divided into 200 000 solid elements and mercury in the pipe was divided into 125 000 solid elements. The interface between the inside of the pipe and mercury was modeled with tied condition. A cut-off pressure model was applied for mercury to simulate the mercury failure due to cavitation [14,15]. In the cut-off pressure model, a relationship between pressure and volumetric strain in mercury is elastic when pressure is larger than a certain value (the cut-off pressure); the mercury has no stiffness when the pressure is less than the cut-off pressure. In this analysis the cut-off pressure of −0.15 MPa was used based on experimental results [16].

4. Experimental results

4.1. Strain response on pipe wall

Fig. 3(a) and (b) shows the strain responses in loop axis and circumference directions, respectively, 50 mm apart from the beam spot. These are all under stagnant mercury condition. Since the

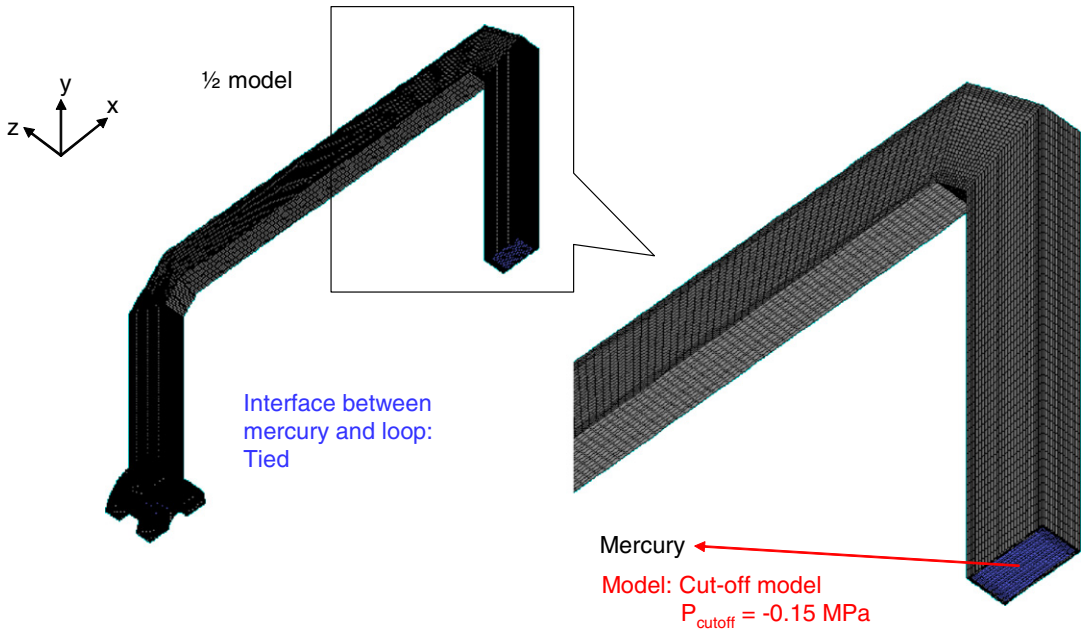

Fig. 2. Numerical analysis model.

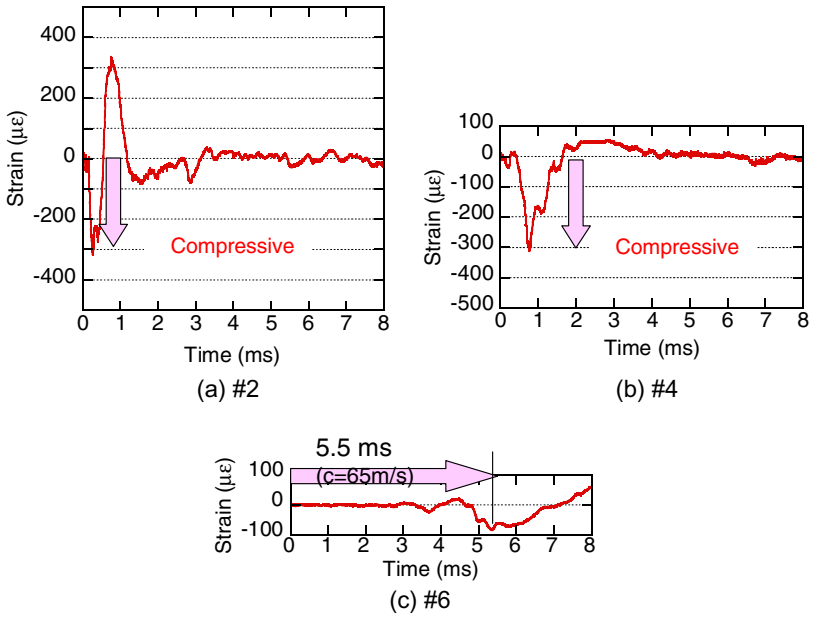

Fig. 3. Strain response obtained in WNR test at (a) strain sensor #2, (b) #4 and (c) #6.

pipe wall is pressurized from the inside of the pipe by the mercury pressure wave, it was expected that the pipe expands and tensile strain is generated on the outer surface of the pipe wall. However, a compressive strain of ca. -300×10^{-6} was first generated at 50 mm apart from beam spot, as shown in Fig. 3(a) and (b). At the sensor #2 the maximum compressive strain in axis direction appeared at 0.2 ms after the proton bombardment while at the sensor #4 the maximum compressive strain of 300×10^{-6} in circumferential direction occurred at 0.7 ms. Fig. 3(c) shows the strain response in circumference direction at 350 mm apart from beam spot (sensor #6). Here, the maximum compressive strain was 90×10^{-6} but it was preceded by a smaller peak of 30×10^{-6}. These occurred at 5.5 ms and 3.8 ms after the proton beam bombardment, respectively. By comparison of the compressive maximums between sensors #4 and #6 and knowledge that they were 300 mm away from each other, the apparent propagation velocity of strain appeared to be 65 m/s. The reduction in magnitude of the compressive strain was from -300×10^{-6} to -100×10^{-6} over this distance.

4.2. Numerical results

Fig. 4(a) and (b) shows the numerical results of strain response corresponding to the same positions shown in Fig. 3(a) and (b), respectively. The numerical results agree well with the experimental results. Fig. 4(c) shows the numerical results of strain response at the same position in Fig. 3(c). As shown in Fig. 3(c), a compressive strain of 90×10^{-6} and preceding small peak of compressive

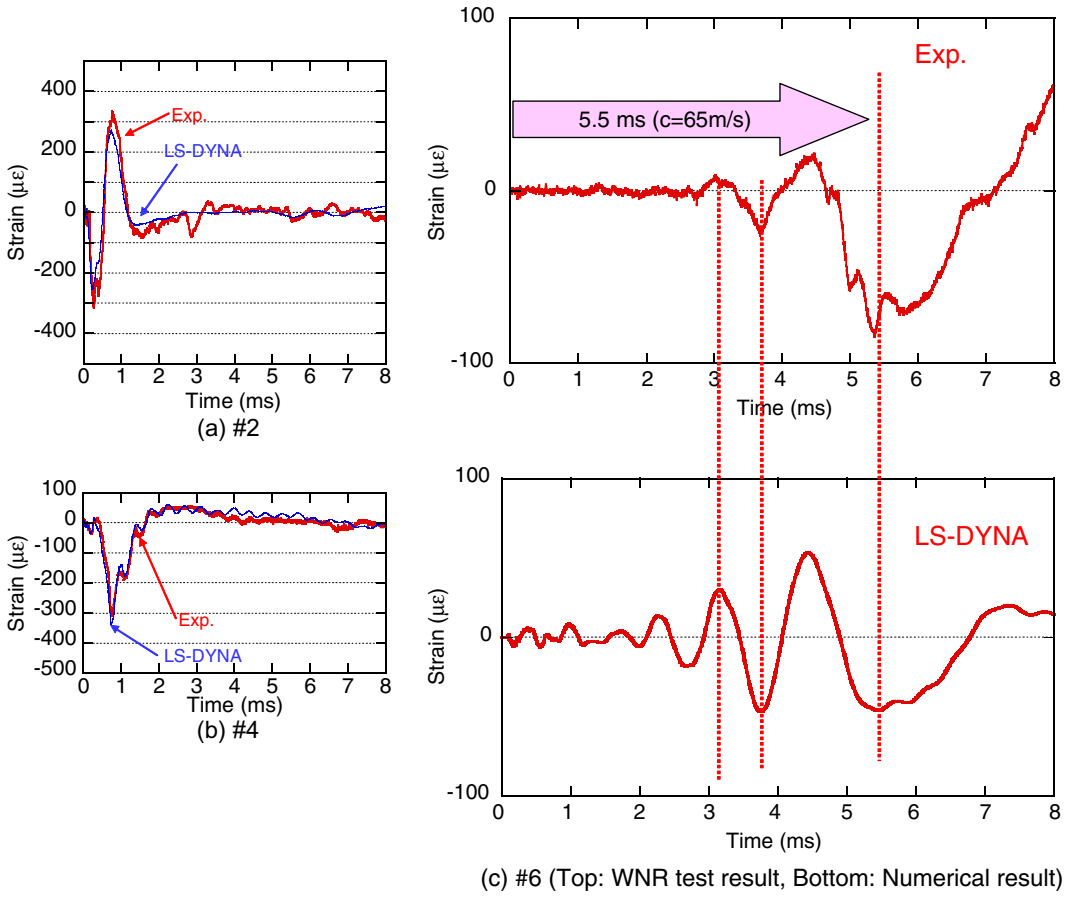

Fig. 4. Comparison of strain response between WNR test result and Numerical result at (a) #2, (b) #4 and (c) #6.

strain of 30×10^{-6} appeared at 5.5 ms and 3.8 ms after the proton beam bombardment, respectively. In the Numerical result, the peaks of the compressive strain also appeared at 3.8 ms and 5.5 ms after proton bombardment.

5. Discussion

5.1. The maximum compressive strain

As shown in Fig. 3(a) and (b), and Fig. 4(a) and (b), the maximum compressive strain appeared. It is important to investigate why the compressive strain appeared in order to understand the pressure wave propagation behavior. Fig. 5(a) shows the history of the strain distribution in pipe axis direction along with the pipe deformation. Up to 0.2 ms after the bombardment, the pipe was expanded by the pressure wave at the beam spot and the tensile strain was generated on the outer surface of the pipe. Later the wall expansion and the tensile strain propagated along the pipe axis. Compressive strain was generated at the front of the strain wave propagation direction due to the deformation of the pipe. This compressive strain was measured at 0.2 ms after the proton bombardment at sensor #2 and followed by tensile strain caused by the expansion of the pipe due to the pressure wave at 0.7 ms.

Fig. 5(b) shows the history of the strain distribution in circumferential direction and pipe deformation. The strain sensor #4 was set near the edge of the rectangular pipe. While the pipe expanded at the beam spot area due to the pressure wave, tensile strain was generated and the compressive strain was generated at the edge of the pipe. As the pressure wave propagated along the pipe axis, the deformation of the pipe was such that tensile circumferential strain occurred near the center of the pipe width while compressive occurred near its edge. Strain sensor #4 caught the compressive strain near the edge generated by this deformation due to the pressure wave. When the circumferential compressive strain was the maximum near the edge, the deflection of the pipe was also maximum. That is, the timing of the compressive strain corresponds to the timing of the pressure wave propagation.

5.2. Propagation of strain wave on the mercury pipe

As shown in Fig. 3(c) and Fig. 4(c), the maximum compressive strain at sensor #6 appeared 5.5 ms after proton bombardment. Since the maximum compressive strain corresponds to the pressure wave propagation, the apparent propagation velocity of the pressure wave is 65 m/s, while the pressure wave propagation velocity in mercury is known to be 1500 m/s.

Fig. 6(a) and (b) shows the diagram of the propagation of the strain response at the edge of the pipe obtained by the numerical simulation up to 0.5 ms and 7.5 ms, respectively. In these Figures, wave fronts are also shown for the steel strain wave (c = 5000 m/s), the pressure wave (c = 1500 m/s) and the apparent propagation velocity of the pressure wave in the rectangular pipe (c = 65 m/s). In Fig. 6a, the strain starts to fluctuate corresponding to the steel strain wave front, although the amplitude is low. So it is understood that the component of strain propagates with the steel strain wave velocity. As shown in Figs. 3(c) and 4(c), the strain at 350 mm away from the beam spot (sensor #6) showed the small peak before arrival of the maximum compressive strain. This is caused by a preceding strain wave by the maximum compressive strain. Fig. 6(b) confirmed that the maximum compressive strain propagates with a velocity of 65 m/s.

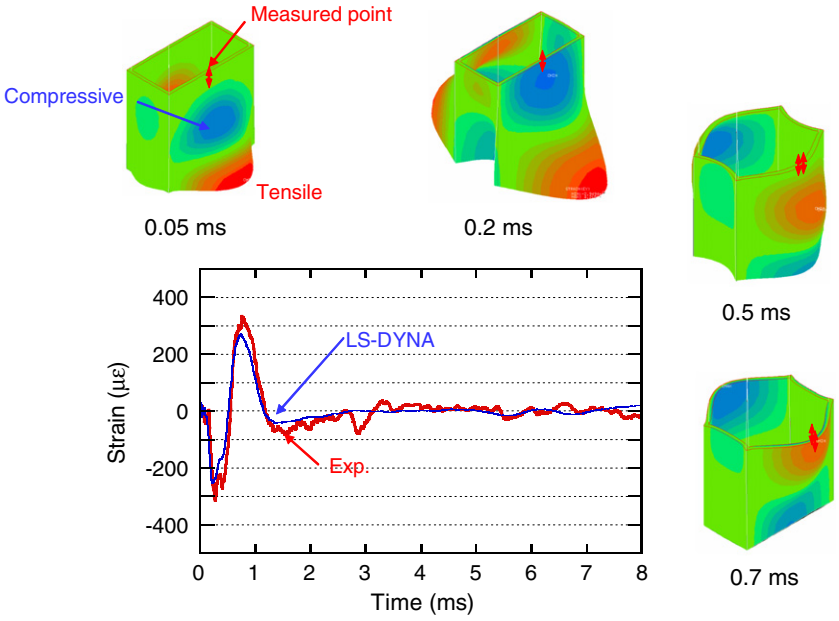

(a) History of deformation and strain distribution in loop axis direction

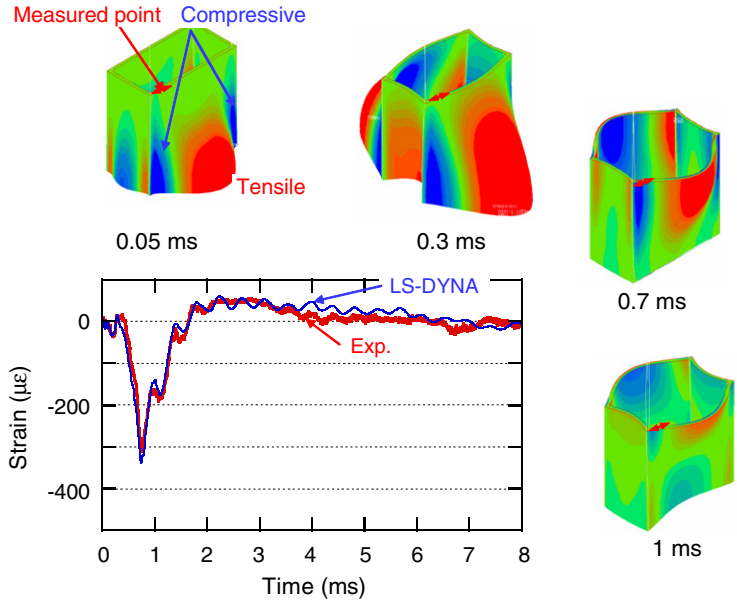

(b) History of deformation and strain distribution in circumference

Fig. 5. History of deformation and strain distribution in (a) loop axis direction and (b) circumference direction.

The propagation velocity of the pressure wave becomes slower in homogeneous gas–liquid two-phase condition [17] or in liquid in elastic pipe [18]. The propagation velocity of the pressure wave in two-phase flow, $c_{\text{two-phase}}$ can be expressed as following [17]

$$c_{\text{two-phase}} = \sqrt{\frac{\kappa P_0}{\rho \alpha_0 (1-\alpha_0)}} \tag{1}$$

where κ is the adiabatic exponent of the gas, P_0 the pressure at the upstream of the pressure wave, ρ the density of the liquid and α_0 the void fraction. The propagation velocity of 65 m/s was obtained under the conditions of P_0 = 0.1 MPaA and α_0 = 0.3%. The possibility to make the homogeneous gas–liquid two-phase condition of 0.3% in the void fraction is low in this test because mercury installed into the IBBTL after vacuuming inside of the loop and there is a fact that the numerical results without effect of the gas agree well with the experimental results.

On the other hand, the apparent propagation velocity of the pressure wave in liquid in circular pipe, c_{elastic} can be estimated from the following [18]

$$c_{\text{elastic}} = \sqrt{\frac{(K_L/\rho)}{(1 + DK_L/tE)}} \tag{2}$$

where K_L is the bulk modulus of liquid, ρ the density of the liquid, D the inner diameter of the pipe, t the thickness of the pipe and E Young's modulus of the pipe material. In short, the velocity is affected by the radial stiffness of the pipe wall. The deflection of the wall consisting the IBBTL's rectangular pipe, w_{IBBTL}, is calculated by following at the center of the wall

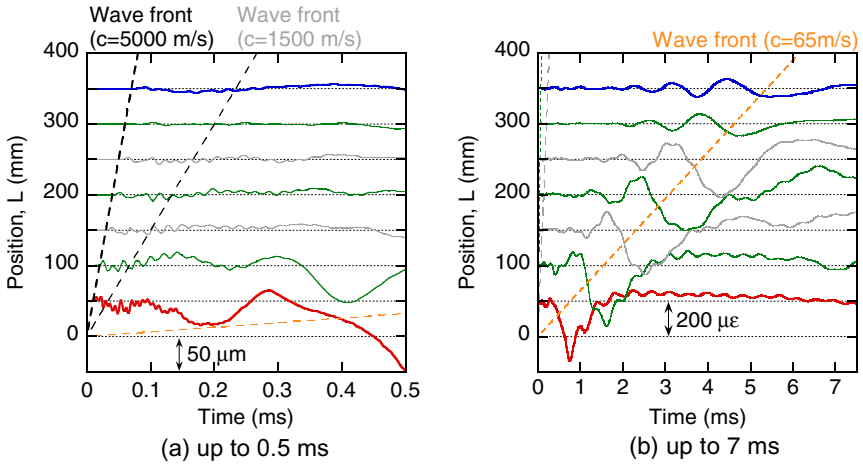

Fig. 6. Diagram of the propagation of strain response in circumference direction at edge up to (a) 0.5 ms and (b) 7 ms.

$$w_{\mathrm{IBBTL}} = \frac{1}{32}\frac{Pb^4}{Et_{\mathrm{IBBTL}}^3} \tag{3}$$

where P is the applied pressure, b the width of the wall, E Young's modulus and t the wall thickness. The displacement of the cylindrical pipe, w_{pipe}, was calculated by following

$$w_{\mathrm{pipe}} = \frac{(2-\nu)R^2}{2Et} \tag{4}$$

where ν is Poisson's ratio, R the inner radius of the pipe. From Eqs. (3) and (4), the wall thickness of the cylindrical pipe, which deforms as similar as the rectangular pipe of IBBTL, was expressed by

$$t = \frac{16(2-\nu)R^2 t_{\mathrm{IBBTL}}^3}{b^4} \tag{5}$$

The rectangular pipe of IBBTL corresponds to the cylindrical pipe of 20 mm in radius from these cross sections. Therefore, the wall thickness of the cylindrical pipe becomes 0.005 mm to deform as similar as the rectangular pipe of IBBTL. The apparent propagation velocity of the pressure wave becomes 65 m/s of this circular pipe. In this calculation, 28.8 GPa and 188 GPa were used as K_{L} and E, respectively.

6. Conclusion

A numerical analysis was carried out by using the FEM code, LS-DYNA, to understand the strain response obtained in the WNR tests in 2005.

The numerical results showed good agreement with the experimental results near the beam spot (sensors #2 and #4). As for the position away from the beam spot (sensor #6), phases agreed well between the experimental and the numerical results. The numerical model, which is also used for JSNS and SNS target design analysis, was verified.

The apparent propagation velocity of the pressure wave becomes low by the interaction between the mercury and the elastic pipe.

References

[1] Planning Division for Neutron Science, in: Proceedings of the 3rd Workshop on Neutron Science Project – Science and Technology in the 21st Century Opened by Intense Spallation Neutron Source, JAERI-Conf 99-003, 1999.
[2] H. Kogawa, et al., in: Proceedings of the ICANS-XVI, vol. III, 2003, p. 1925.
[3] S. Ishikura, H. Kogawa, M. Futakawa, et al., Kouon-gakkai shi 28 (6) (2002) 329 (in Japanese).
[4] M. Futakawa, H. Kogawa, R. Hino, J. Phys. IV France 10 (Pr9) (2000) 237.
[5] M. Futakwa, H. Kogawa, Y. Midorikawa, R. Hino, H. Date, H. Takeishi, in: Proceedings of the 4th Int. Symp. Imp. Eng., 2001, p. 339.
[6] M. Futakawa, H. Kogawa, R. Hino, H. Date, H. Takeishi, Int. J. Impact Eng. 28 (2003) 123.
[7] M. Futakawa, T. Naoe, H. Kogawa, C.C. Tsai, Y. Ikeda, J. Nucl. Sci. Technol. 40 (2003) 895.
[8] M. Futakawa, T. Naoe, C.C. Tsai, H. Kogawa, S. Ishikura, Y. Ikeda, H. Soyama, H. Date, J. Nucl. Mater. 343 (2005) 70.
[9] M. Futakawa, T. Naoe, H. Kogawa, Y. Ikeda, J. Nucl. Sci. Technol. 41 (2004) 1059.
[10] H. Soltner, ESS 03-152-T, 2003.
[11] K. Okita, S. Takagi, Y. Matsumoto, Nihon Kikai Gakkai Ronbunsyu B 72 (716) (2006) 885 (in Japanese).
[12] B. Riemer, in these proceedings.
[13] Livermore Software Technology Corp., LS-DYNA, 1998.
[14] B. Riemer, J. Nucl. Mater. 343 (2005) 81.
[15] H. Kogawa, M. Futakawa, S. Ishikura, J. Nucl. Sci. Technol. 44 (2007) 523.
[16] T. Naoe, M. Futakawa, T. Koyama, H. Kogawa, Jikken Rikigaku 6 (2006) 301 (in Japanes).
[17] K. Hijikata, Y. Mori, Y. Takahashi, Nucl. Eng. Des. 95 (1986) 343.
[18] N. Ogawa, Report of the National Research Institute for Earth Science and Disaster Prevention, vol. 15, 1976, pp. 57–73 (in Japanes).